Nonlinear dynamics in the resonance line shape of NbN superconducting resonators

B. Abdo,* E. Segev, O. Shtempluck, and E. Buks
Microelectronics Research Center, Department of Electrical Engineering, Technion, Haifa 32000, Israel
(Received 23 May 2005; revised manuscript received 5 December 2005; published 17 April 2006)

We report on unusual nonlinear dynamics observed in the resonance response of NbN superconducting microwave resonators. The nonlinear dynamics which occurs at relatively low input powers (2–4 orders of magnitude lower than Nb) includes among others, jumps in the resonance line shape, hysteresis loops changing direction, and resonance frequency shift. These effects are measured herein using varying input power, applied magnetic field, white noise, and rapid frequency sweeps. Based on these measurement results, we consider a hypothesis according to which local heating of weak links forming at the boundaries of the NbN grains is responsible for the observed behavior, and we show that most of the experimental results are qualitatively consistent with such a hypothesis.

DOI: 10.1103/PhysRevB.73.134513 PACS number(s): 74.50.+r, 85.25.−j, 47.20.Ky, 05.45.Xt

I. INTRODUCTION

Understanding the underlying mechanisms that cause and manifest nonlinear effects in superconductors has a significant implications for both basic science and technology. Nonlinear effects in superconductors may be exploited to demonstrate some important quantum phenomena in the microwave regime as was shown in Refs. 1 and 2 and as was suggested recently in Refs. 3 and 4, whereas, technologically, these effects, in general, can play a positive or negative role depending on the application. On the one hand, they are very useful in a wide range of nonlinear devices such as amplifiers,[5,6] mixers,[7] single-photon detectors,[8] and superconducting quantum interference devices (SQUID's).[9] On the other hand, in other applications mainly in the telecommunication area, such as bandpass filters and high-Q resonators, nonlinearities are highly undesirable.[10–13]

Various nonlinear effects in superconductors and in NbN in particular have been reported and analyzed in the past by several research groups. Duffing-like nonlinearity, for example, was observed in superconducting resonators employing different geometries and materials. It was observed in a high-T_c superconducting (HTS) parallel-plate resonator,[14] in a Nb microstrip resonator,[15] in Nb and NbN stripline resonators,[13] in a YBCO coplanar-waveguide resonator,[16] in a YBCO thin-film dielectric cavity,[17] and also in a suspended HTS thin-film resonator.[18] Other nonlinearities including notches, anomalies developing at the resonance line shape, and frequency hysteresis were reported in Refs. 19–21.

However, in spite of the intensive study of nonlinearities in superconductors in the past decades and the great progress achieved in this field, the determination of the underlying mechanisms responsible for the microwave nonlinear behavior of both low- and high-T_c superconductors is in many experiments still a subject of debate.[22] This is partly because of the variety of preparation and characterization techniques employed and the numerous fabrication parameters involved. In addition nonlinear mechanisms in superconductors, which are usually divided into intrinsic and extrinsic, are various and many times act concurrently. Thus identifying the dominant mechanism is in general difficult.[23]

Among the nonlinear mechanisms investigated in superconductors one can name the Meissner effect,[24] pair-breaking, global, and local heating effects,[14,17] rf and dc vortex penetration and motion,[25] defect points, damaged edges,[26] substrate material,[27] and weak links (WL's),[28] where WL is a collective term which represents various material defects such as weak superconducting points switching to normal state under low current density, Josephson junctions forming inside the superconductor structure, grain boundaries, voids, insulating oxides, and insulating planes. These defects and impurities generally affect the conduction properties of the superconductor and as a result cause extrinsic nonlinear effects.

In this paper we report the observation of unique nonlinear effects measured in the resonance line shape of NbN superconducting microwave resonators. Among the observed effects are asymmetric resonances, multiple jumps in the resonance curve, hysteretic behavior in the vicinity of the jumps, frequency hysteresis loops changing direction, jump frequency shift as the input power is increased, and nonlinear coupling. Some of these nonlinear effects were introduced by us in a previous publication.[29] Thus this paper will focus on presenting a more current set of measurements applied to these nonlinear resonators, which provides a better understanding of the underlying physical mechanism causing these effects. To this end, we have measured the nonlinear superconducting resonators using different operating conditions, such as bidirectional frequency sweeps, added white noise, fast frequency sweep using frequency modulation (FM), and dc magnetic fields. In each case we observe a unique nonlinear dynamics of the resonance line shape which is qualitatively different from the commonly reported Duffing oscillator nonlinearity. We attribute these nonlinear effects to WL's forming at the boundaries of the NbN columnar structure. A theoretical model explaining the dynamical behavior of the resonance line shape in terms of abrupt changes in the macroscopic parameters of the resonator, due to local heating, is formulated. Furthermore, simulations based on this model are shown to be in very good qualitative agreement with the experimental results.

The remainder of this paper is organized as follows: The fabrication process of the NbN superconducting resonators is described briefly in Sec. II. The nonlinear response of these resonators measured using various operating conditions are

 ©2006 The American Physical Society

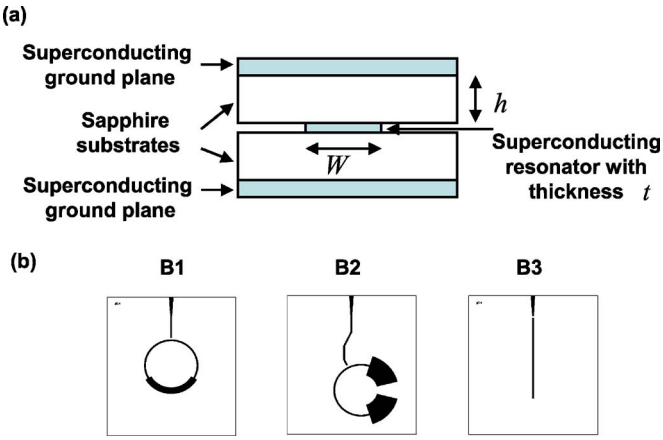

FIG. 1. (Color online). (a) Schematic cross section of the stripline geometry used, which consists of five layers: two superconducting ground planes, two sapphire substrates, and a NbN film in the middle deposited on one of the sapphires. (b) Top view of the three resonator layouts (B1, B2, B3) which were deposited as the center layer.

reviewed in Sec. III. A comparison with other nonlinearities reported in the literature is given in Sec. IV. The possible underlying physical mechanisms responsible for the observed effects are discussed in Sec. V, whereas in Sec. VI, a theoretical model based on local heating of weak links is suggested, followed by simulations which qualitatively reproduce most of the nonlinear features observed in the experiments. Finally, in Sec. VII, a short summary concludes this paper.

II. FABRICATION PROCESS

The measurement results presented in this paper belong to three nonlinear NbN superconducting microwave resonators. The resonators were fabricated using stripline geometry, which consists of two superconducting ground planes, two sapphire substrates, and a center strip deposited in the middle (the deposition was done on one of the sapphire substrates). Figure 1 shows a schematic diagram illustrating stripline geometry and a top view of the three resonator layouts. We will refer to the three resonators in the text by the names B1, B2 and B3 as defined in Fig. 1. The dimensions of the sapphire substrates used were 34 mm$\times$30 mm$\times$1 mm, whereas the coupling gap between the resonators and their feedline was set to 0.4 mm in the B1 and B3 and 0.5 mm in the B2 resonators. The resonators were dc magnetron sputtered in a mixed Ar/N_2 atmosphere, near room temperature. The patterning was done using the standard UV photolithography process, whereas the NbN etching was performed by Ar-ion milling. The sputtering parameters and design considerations as well as physical properties of the NbN films can be found elsewhere.[29] The critical temperature T_c of the B1, B2, and B3 resonators was relatively low and equal to 10.7 K, 6.8 K, and 8.9 K, respectively. The thickness of the NbN resonators was 2200 Å in the B1, 3000 Å in the B2, and 2000 Å in the B3 resonators.

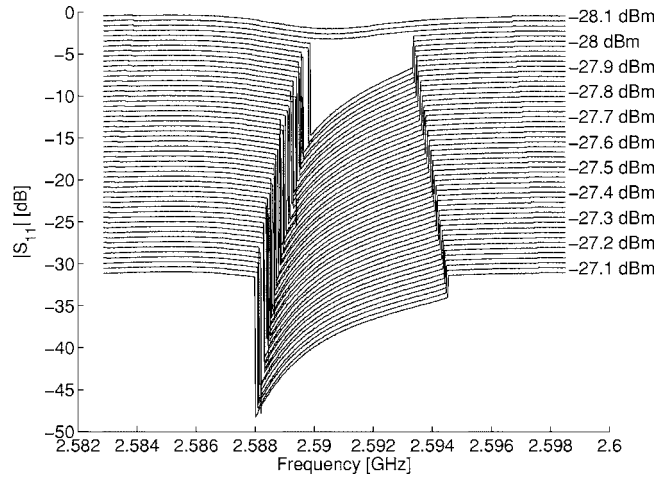

FIG. 2. S_{11} amplitude measurement of the B1 resonator at its first mode. The measured resonance line shapes are asymmetrical and contain two abrupt jumps at the sides of the resonance. Moreover, the jump frequencies shift outwards as the input power is increased. The measured resonance line shapes were shifted vertically by a constant offset for clarity.

III. NONLINEAR RESONANCE RESPONSE

In the following subsections, we present experimental results emphasizing the different aspects of the nonlinear response exhibited by the B1, B2, and B3 resonators. In Sec. III A, a resonance response measurement obtained while varying the input rf power is presented, showing an abrupt and low-power onset of nonlinearity. In Secs. III B–III D,, representative experimental results measured while scanning the resonance response in the forward and backward directions are shown, exhibiting, respectively, hysteresis loops changing direction, metastability, and multiple jumps, whereas in Sec. III E, the dependence of the resonance line shape on the applied dc magnetic field is examined, where the resonance line shape exhibits a change in the direction of the jump and vanishing jump features. All measurements presented were performed at liquid-helium temperature 4.2 K.

A. Abrupt onset of nonlinearity

In Fig. 2 we present a S_{11} parameter measurement of the B1 first mode using a vector network analyzer. At low input powers, the resonance response line shape is Lorentzian and symmetrical. As the input power is increased gradually in steps of 0.01 dBm, the resonance response changes dramatically and abruptly at about −28.04 dBm. It becomes extremely asymmetrical and includes two abrupt jumps at both sides of the resonance line shape. The magnitude of the jumps at some input powers can be as high as 16 dB. As the input power is increased the resonance frequency is red-shifted and the jump frequencies shift outwards away from the center frequency. Moreover, at much higher powers not shown in the figure, the resonance curve becomes gradually shallower and broader in the frequency span. It is also worthwhile noting that the intensive evolution of the resonance

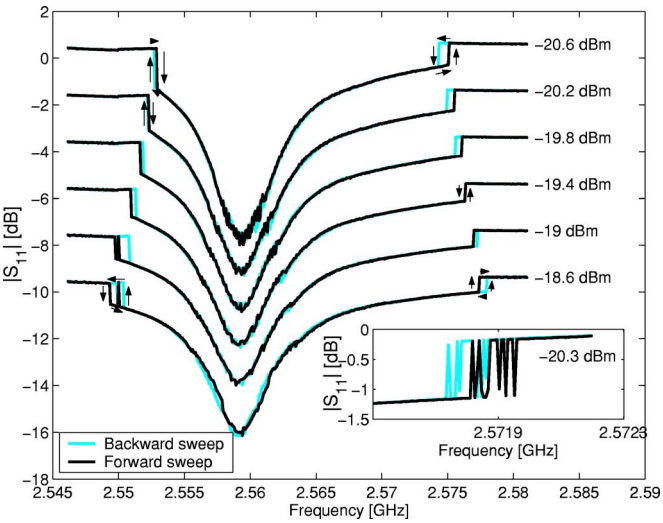

FIG. 3. (Color online). Frequency sweep measurement of the B1 resonator at its first mode performed in both frequency directions. The plots exhibit hysteresis loops forming at the vicinity of the jumps and hysteresis loops changing direction as the input power is increased. The black line represents a forward sweep, whereas the cyan (gray) line represents a backward sweep. The number of measurement points employed in each scan direction is 500 points. The resonance line shapes were shifted vertically by a constant offset for clarity. In the inset, a "zoom-in" measurement of the right hysteresis loop of the B1 first resonance is shown. The measurement, which was obtained using a spectrum analyzer, includes 100 data points and corresponds to −20.3 dBm input power.

line shape shown in Fig. 2 takes place within only a 1-dBm power range.

B. Hysteretic behavior

As the response function for nonlinear systems becomes multiple valued or lacks a steady-state solution in some parameter domain, nonlinear systems tend to demonstrate hysteretic behavior with respect to that parameter.

Frequency hysteresis in the resonance line shape of superconducting resonators exhibiting Duffing oscillator nonlinearity and other kinds of nonlinearities was observed by several groups.[19,30] Hysteretic behavior and losses in superconductors were discussed also in Refs. 25 and 31. Moreover, recent works, which examined the resonance response of a rf tank circuit coupled to a SQUID, have reported several interesting frequency hysteresis features.[32–34]

Likewise, measuring the resonance response of our nonlinear resonators yields a hysteretic behavior in the vicinity of the jumps. However, this hysteretic behavior is unique in many aspects. In Fig. 3 we show a S_{11} measurement of the B1 resonator at its first mode, measured while sweeping the frequency in both directions. The input power range shown in this measurement corresponds to a higher-power range than that of Fig. 2. The black line represents a forward frequency sweep, whereas the cyan (gray) line represents a backward frequency sweep.

At −20.6 dBm the resonance line shape contains two jumps in each scan direction and two hysteresis loops. The left hysteresis loop circulates clockwise whereas the right loop circulates counterclockwise. However, the common property characterizing them is that the jumps occur at higher frequencies in the forward scan compared to their counterparts in the backward scan. As the input power is increased to about −20.2 dBm the two opposed jumps at the left side meet and the left hysteresis loop vanishes. At about −19.4 dBm a similar effect happens to the right hysteresis loop, and it vanishes as well, whereas at higher input powers (i.e., −19 dBm, −18.6 dBm) the two jumps occur earlier at each frequency sweep direction, causing the hysteresis loops to appear circulating in the opposite direction compared to the −20.6-dBm resonance curve, for instance. As we show in the next subsection, this picture of well-defined hysteresis loops is strongly dependent on the applied frequency sweep rate and on the system noise. A possible explanation for this unique hysteretic behavior would be presented in Sec. VI.

C. Metastable states

Jumps in the resonance response of a nonlinear oscillator are usually described in terms of metastable and stable states and the dynamic transition between basins of attraction of the oscillator;[35] thus in order to examine the stability of these observed resonance jumps, we carried out several measurements.

In one measurement, we have "zoomed in" around the right jump of the resonance at −20.3 dBm and examined its frequency response in both directions. The measurement setup included a signal generator, the cooled resonator, and a spectrum analyzer. The reflected signal power off the resonator was redirected by a circulator and measured using a spectrum analyzer. The measurement result obtained using 100 sampling points in each direction is exhibited in the inset of Fig. 3, where the metastable nature of the jump region is clearly demonstrated.

In another measurement configuration we have investigated this metastability further by monitoring the effect of applied broadband noise on the resonance jumps. We applied a constant white-noise power to the resonator, several orders of magnitude lower than the main signal power. The applied white noise level was −58 dBm/Hz (measured separately using spectrum analyzer) and was generated by amplifying the thermal noise of a room-temperature 50-Ω load using an amplifying stage. The generated noise was added to the transmitted power of a network analyzer via a power combiner. The reflected power was redirected by a circulator and was measured at the second port of the network analyzer. The effect of the −58-dBm/Hz white-noise power on the B1 first-mode jumps is shown in Fig. 4(a), whereas in Fig. 4(b) we show for comparison the nearly noiseless case obtained after disconnecting the amplifier and combiner stage. The two measurements were carried out within the same input power range (from −23.9 dBm to −20 dBm).

By comparing the two measurement results, one can make the following observations. The twofold jumps in Fig. 4(b) form a hysteresis loop at both sides of the resonance curve. By contrast in Fig. 4(a), as a result of the added noise, the hysteresis loops at the right side vanish, while the jumps at

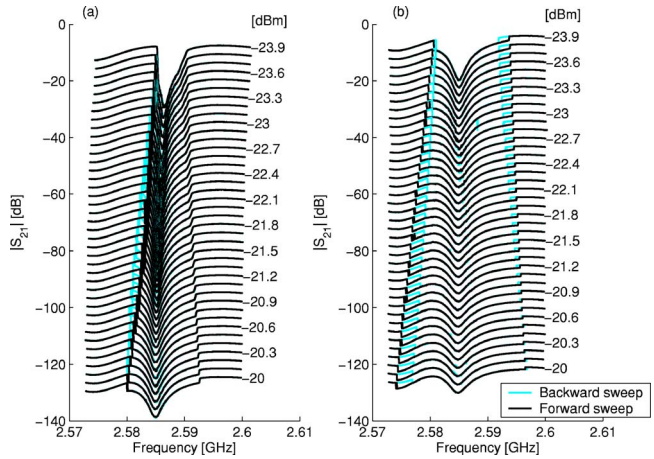

FIG. 4. (Color online). Frequency sweep measurement of the B1 resonator first mode performed in both directions while (a) applying white noise of −58 dBm/Hz (b) without applying external noise. The black line represents a forward sweep, whereas the cyan (gray) line represents a backward sweep. The measured resonance curves were shifted vertically by a constant offset for clarity.

the left side become frequent and bidirectional (indicated by the thick colored lines).

At a given input drive, the transition rate $\Gamma(f)$ between the oscillator basins of attraction can be generally estimated by the expression $\Gamma(f)=\Gamma_0\exp(-E_A(f)/k_BT_{eff})$,[35] where $E_A(f)$ is the quasiactivation energy of the oscillator, T_{eff} is proportional to the noise power, k_B is Boltzmann's constant, and f is the oscillator frequency, whereas Γ_0 is related to Kramers low-dissipation form[36] and it is given approximately by f_0/Q, where f_0 is the natural resonance frequency and Q is the quality factor of the oscillator. From our results we roughly estimate the order of magnitude of E_A to be 10^{14} K for the jump on the left.[35] Note, however, that this quantity varies for different transitions and strongly depends on the operating point.

D. Multiple jumps

Another nonlinear feature—namely, multiple jumps in the resonance line shape—is observed in the resonance response of B3, while sweeping the frequency in the forward and backward directions. In Fig. 5 we show a representative measurement of the first resonance of B3 corresponding to 1.49 dBm input power, exhibiting three jumps in each sweep direction and four hysteresis loops.

E. dc magnetic field dependence

Measuring the B2 resonator second mode under a dc magnetic field yielded additional nonlinear features in the resonance response line shape as shown in Figs. 6 and 7.

In Fig. 6 we show the resonance line shape of the B2 second mode measured while applying a perpendicular dc magnetic field of 90 mT. As the input rf power is increased gradually, the resonance line shape undergoes different phases. While at low and high powers the curves are Lorentzians and symmetrical, in the intermediate range, the resonance curves include a jump at the left side, which, as the input power increases, flips from the upward to the downward direction.

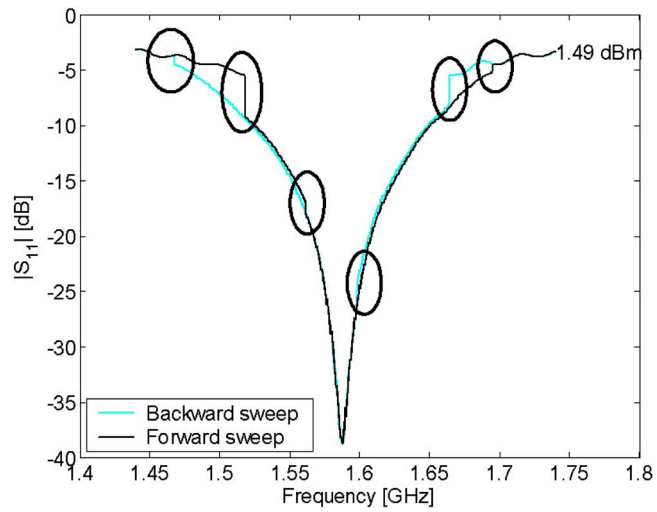

FIG. 5. (Color online). S_{11} amplitude measurement of the first resonance of the B3 resonator, measured at an input power of 1.49 dBm. The measurement was done using a network analyzer employing 4000 measurement points in each direction. The black line represents a forward frequency scan whereas the cyan (gray) line represents a backward frequency scan. The plot shows clearly three jumps within the resonance line shape in each direction, as indicated by small circles.

In Fig. 7, where we have set a constant input power of −5 dBm and increased the applied magnetic field by small steps, the left-side jump vanishes as the magnetic field exceeds some relatively low threshold of ~11.8 mT. These effects will be further discussed in Secs. V and VI.

IV. COMPARISON WITH OTHER NONLINEARITIES

The most commonly reported nonlinearity in superconductors is the Duffing oscillator nonlinearity. However, this

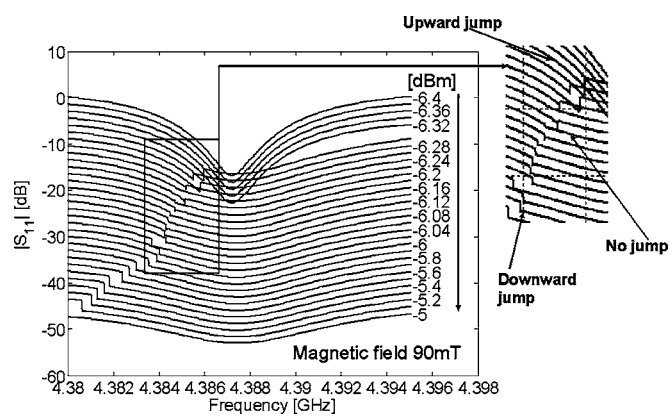

FIG. 6. B2 nonlinear resonance response measured under a constant magnetic field of 90 mT while increasing the input power. The resonance which starts as a Lorentzian at low powers, develops into a resonance curve having an upward jump, a curve with no jump, a curve having a downward jump, and finally a Lorentzian curve again as the power is increased. The measured curves were shifted vertically by a constant offset for clarity.

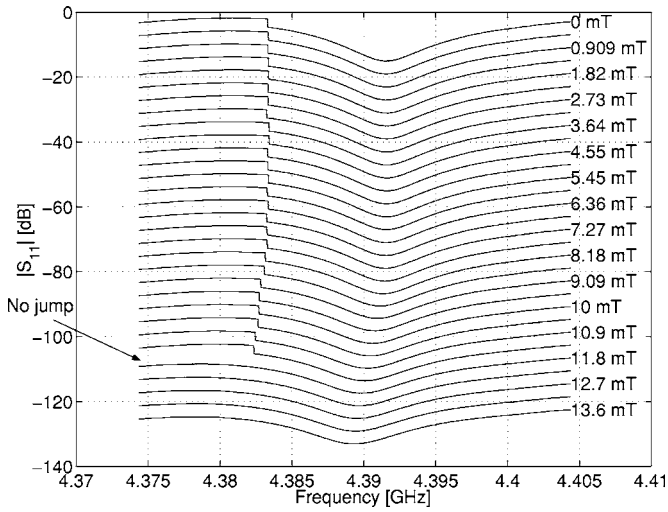

FIG. 7. Increasing the magnetic field gradually from zero while applying a constant input power level of −5 dBm causes the jump in the B2 resonance line shape to disappear at a relatively low value of 11.8 mT. This vanishing jump indicates that the jump mechanism is sensitive to the magnetic field. The measured curves were shifted vertically by a constant offset for clarity.

nonlinearity is qualitatively different from the nonlinearity we observe in our NbN samples and which is reported in this paper. In Fig. 8 we show, for the sake of visual comparison, a resonance response measured at 4.2 K, exhibiting Duffing oscillator nonlinearity of the kind generally reported in the literature.[13,14,16] This nonlinearity, which can be explained in terms of resistance change ΔR and kinetic inductance change ΔL_K,[10,30,37] was measured at the first resonance frequency of a 2200-Å-thick Nb resonator employing B2 layout geometry (T_c=8.9 K). The differences between the two nonlinear dynamics shown in Figs. 2 and 8 are obvious. In Fig. 8 the nonlinearity is gradual, while in Fig. 2 the power onset of nonlinearity is abrupt and sudden. In Fig. 8, the resonance response in the nonlinear regime contains an infinite slope at the left side, whereas in Fig. 2 the curves contain two jumps at both sides of the resonance response. In Fig. 8 changes in the resonance curve are measured on a power scale of 1 dBm, while changes in Fig. 2 are measured on a 0.01 dBm power scale. Whereas the onset of nonlinearity in Fig. 8 is on the order of 10 dBm, the onset of nonlinearity in Fig. 2 is about 4 orders of magnitude lower, ∼−28 dBm. Furthermore, the presented nonlinearity differs from Duffing oscillator nonlinearity in its hysteretic behavior and its multiple-jump feature shown in Fig. 5.

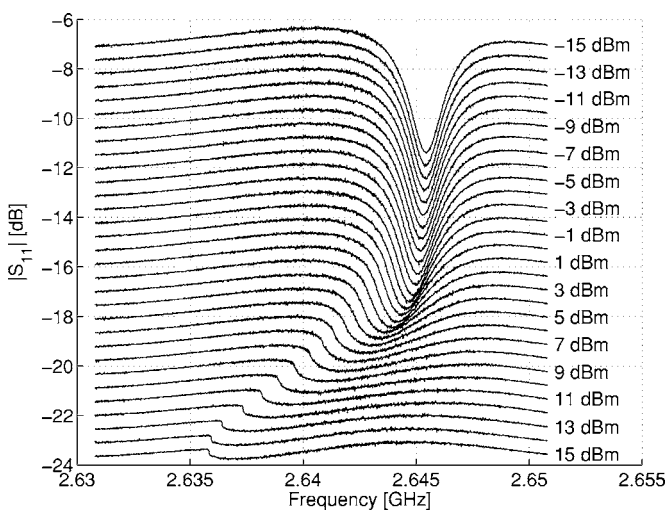

FIG. 8. Duffing oscillator nonlinearity exhibited by a Nb stripline resonator employing a B2 layout at its first mode. The different plots of the S_{11} amplitude correspond to different input powers, ranging from −15 dBm to 15 dBm in steps of 1 dBm. As the input power is increased the resonance becomes asymmetrical and an infinite slope builds up at the left side of the resonance curve. The plots were offset in the vertical direction for clarity.

Abrupt jumps in the resonance line shape, similar in some aspects to the jumps reported herein, were observed in two-port high-T_c YBCO resonators.[19–21] Portis *et al.*[19] have also reported some frequency hysteretic behavior in the vicinity of the jumps. However, one significant difference between the two nonlinearities is the onset power of nonlinearity reported in these references, which is on the order of 20 dBm[20,21]—that is, about 5 orders of magnitude higher than the onset power of nonlinearity of the B1 first mode (∼−28 dBm). All three works[19–21] have attributed the nonlinear abrupt jumps to local heating of distributed WL's in the resonator film.

V. POSSIBLE NONLINEAR MECHANISMS

The relatively very low power onset of nonlinearity observed in these resonators as well as its strong sensitivity to rf power highly implies an extrinsic origin of these effects, and as such, hot spots in WL's are a leading candidate for explaining the nonlinearity.

Vortex penetration in the bulk or in WL's is less likely, mainly because heating the sample above T_c between sequential magnetic field measurements has yielded reproducible results with good accuracy in the magnetic field magnitude, the microwave input power, and the jump frequency (less than 200 kHz offset). Moreover, the low-magnetic-field threshold ∼11.8 mT above which the B2 resonance jump vanished is about 3.5 times lower than the H_{c_1} (flux penetration) of NbN reported, for example, in Ref. 13.

In the following subsection, Sec. V A, we provide a direct evidence of WL, whereas in Sec. V B, we exclude the global heating mechanism as a possible source of the nonlinearities.

A. Columnar structure

It is well known from numerous research works done in the past[38,39] that NbN films can grow in a granular columnar structure under certain deposition conditions. Such columnar structure may even promote the growth of random WL's at the grain boundaries of the NbN films. To examine the NbN structure we have sputtered about a 2200-Å NbN film on a thin small rectangular sapphire substrate of 0.2 mm thickness. The sputtering conditions applied were similar to those used in the fabrication of the B2 resonator. Following the sputtering process, the thin sapphire was cleaved and a scan-

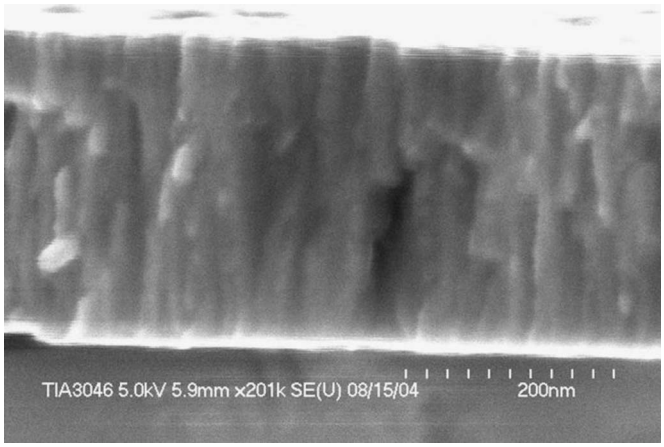

FIG. 9. A SEM micrograph showing a 2200-Å NbN film deposited on a thin sapphire substrate using similar sputtering conditions as the B2 resonator. The micrograph exhibits clearly the columnar structure of the NbN film and its grain boundaries.

ning electron microscope (SEM) micrograph was taken at the cleavage plane. The SEM micrograph appearing in Fig. 9, which shows clearly the columnar structure of the deposited NbN film and its grain boundaries, further supports the weak-link hypothesis. The typical diameter of each NbN column is about 20 nm.

B. Frequency sweep time analysis

Resistive losses and heating effects are typically characterized by relatively long time scales.[14] In an attempt to consider whether such effects are responsible for the observed nonlinearities in general and for the jumps in particular, we have run a frequency sweep time analysis using the experimental setup depicted in Fig. 10. We have controlled the frequency sweep cycle of a signal generator via FM modulation. The FM modulation was obtained by feeding the signal generator with a sawtooth wave form of $1/f$ sweep time cycle. The reflected power off the resonator was redirected

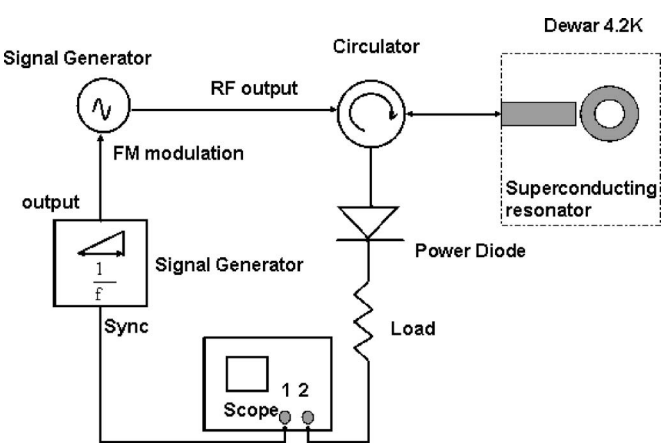

FIG. 10. Frequency sweep time analysis setup. The frequency sweep time of the microwave signal generator was FM modulated by a sawtooth wave form of frequency f. The reflected power off the resonator was measured by a power diode and an oscilloscope.

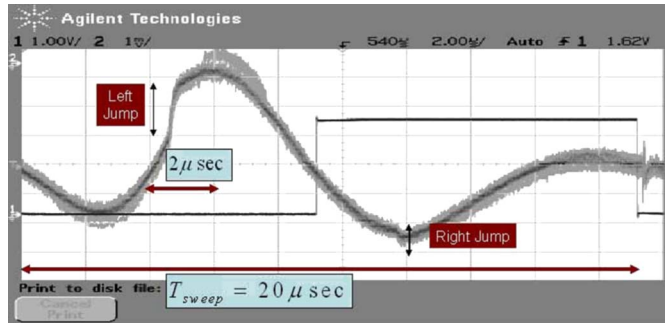

FIG. 11. (Color online). Frequency sweep time measurement. The figure displays the resonance measured by an oscilloscope while applying a sawtooth FM modulation of frequency 50 kHz (T_{sweep}=20 μs) to the signal generator. The left and right jumps of the resonance are still apparent in spite of the fast rate frequency sweep. Thus indicating that the jumps do not originate from any global heating mechanism.

using a circulator and measured by a power diode and an oscilloscope. The left- and right-hand jumps of B2 ~4.39 GHz resonance were measured using this setup, while applying increasing FM modulation frequencies up to 200 kHz. In Fig. 11 we present a measurement result obtained at 50 kHz FM modulation or, alternatively, T_{sweep} of 20 μs. The FM modulation applied was ±20 MHz around the center frequency 4.4022 GHz. The measured resonance response appears inverted in the figure due to the negative output polarity of the power diode. The fact that both jumps continue to occur within the resonance line shape (see Fig. 11), in spite of the short duty cycles that are of the order of $\sim\mu s$, indicates that heating processes which have typical time scales on the order of s to ms (Ref. 14) are unlikely to cause these effects.

However, the above measurement result does not exclude local heating of WL's.[40–42] Assuming that the substrate is isothermal and that the hot spot is dissipated mainly down into the substrate rather than along the film,[40] one can evaluate the characteristic relaxation time of the hot spot using the equation $\tau = Cd/\alpha$, where C is the heat capacity of the superconducting film (per unit volume), d is the film thickness, and α is the thermal surface conductance between the film and substrate.[41] Substituting for our B2 NbN resonator yields a characteristic relaxation time of $\tau \simeq 5.4 \times 10^{-8}$ s, where the parameters $C \simeq 2.7 \times 10^{-3}$ J cm^{-3} K^{-1} (NbN),[42] $d = 3000$ Å (B2 thickness), and $\alpha \simeq 1.5$ W cm^{-2} K^{-1} at 4.2 K (sapphire substrate)[42] have been used. A similar calculation based on values given in Ref. 40 yields $\tau \simeq 2.1 \times 10^{-9}$ s. These time scales are of course 2–3 orders of magnitude lower than the time scales examined by the FM modulation setup, and thus local heating of WL's is not ruled out.

VI. LOCAL HEATING MODEL

In this section we consider a hypothesis according to which local heating of WL's is responsible for the observed effects. We show that this hypothesis can account for the main nonlinear features observed and that simulations based

on such a theoretical model exhibit a very good qualitative agreement with the experimental results.

A. Theoretical modeling

Consider a resonator driven by a weakly coupled feedline carrying an incident coherent tone $b^{in}e^{-i\omega_p t}$, where b^{in} is a constant complex amplitude and ω_p is the drive angular frequency. The mode amplitude inside the resonator A can be written as $A=Be^{-i\omega_p t}$, where $B(t)$ is a complex amplitude, which is assumed to vary slowly on the time scale of $1/\omega_p$. In this approximation, the equation of motion of B reads[3]

$$\frac{dB}{dt} = [i(\omega_p - \omega_0) - \gamma]B - i\sqrt{2\gamma_1}b^{in} + c^{in}, \tag{1}$$

where ω_0 is the angular resonance frequency, $\gamma=\gamma_1+\gamma_2$, γ_1 is the coupling constant between the resonator and feedline, and γ_2 is the damping rate of the mode. The term c^{in} represents input noise with vanishing average

$$\langle c^{in}\rangle = 0 \tag{2}$$

and correlation function given by

$$\langle c^{in}(t)c^{in*}(t')\rangle = G\omega_0\delta(t-t'). \tag{3}$$

In thermal equilibrium and for the case of high temperature $k_BT \gg \hbar\omega_0$, where k_B is Boltzmann's constant, one has

$$G = \frac{2\gamma}{\omega_0}\frac{k_BT}{\hbar\omega_0}. \tag{4}$$

In terms of the dimensionless time $\tau=\omega_0 t$, Eq. (1) reads

$$\frac{dB}{d\tau} = \frac{i(\omega_p-\omega_0)-\gamma}{\omega_0}(B-B_\infty) + \frac{c^{in}}{\omega_0}, \tag{5}$$

where

$$B_\infty = \frac{i\sqrt{2\gamma_1}b^{in}}{i(\omega_p-\omega_0)-\gamma}. \tag{6}$$

Small noise gives rise to fluctuations around the steady-state solution B_∞. A straightforward calculation yields

$$\langle |B-B_\infty|^2\rangle = \frac{G\omega_0}{2\gamma}. \tag{7}$$

The output signal a^{out} reflected off the resonator can be written as $a^{out}=b^{out}e^{-i\omega_p t}$. The input-output relation relating the output signal to the input signal is given by[43]

$$\frac{b^{out}}{\sqrt{\omega_0}} = \frac{b^{in}}{\sqrt{\omega_0}} - i\sqrt{\frac{2\gamma_1}{\omega_0}}B, \tag{8}$$

whereas the total power dissipated in the resonator Q_t can be expressed as[3]

$$Q_t = \hbar\,\omega_0 2\gamma_2 E, \tag{9}$$

where $E=|B|^2$.

Furthermore, consider the case where the nonlinearity is originated by a local hot spot in the stripline resonator. If the hot spot is assumed to be sufficiently small, its temperature T can be considered to be homogeneous. The temperature of the other parts of the resonator is assumed to be equal to that of the coolant, T_0. The power Q heating up the hot spot is given by $Q=\alpha Q_t$ where $0\leqslant\alpha\leqslant 1$.

The heat balance equation reads

$$C\frac{dT}{dt} = Q - W, \tag{10}$$

where C is the thermal heat capacity, $W=H(T-T_0)$ is the heat power transferred to the coolant, and H is the heat transfer coefficient. Defining the dimensionless temperature[44]

$$\Theta = \frac{T-T_0}{T_c-T_0}, \tag{11}$$

where T_c is the critical temperature, one has

$$\frac{d\Theta}{d\tau} = -g(\Theta-\Theta_\infty), \tag{12}$$

where

$$\Theta_\infty = \frac{2\alpha\gamma_2\rho E}{\omega_0 g}, \tag{13}$$

$$\rho = \frac{\hbar\omega_0}{C(T_c-T_0)}, \tag{14}$$

$$g = \frac{H}{C\omega_0}. \tag{15}$$

While in Duffing oscillator equation discussed in Ref. 3 the nonlinearity can be described in terms of a gradually varying resonance frequency which depends on the amplitude of the oscillations inside the cavity, in the current case, the resonance frequency ω_0, the damping rates γ_1 and γ_2, and the α factor are considered to have a step function dependence on T, the temperature of the WL's:

$$\omega_0 = \begin{cases} \omega_{0s} & \Theta < 1, \\ \omega_{0n} & \Theta > 1, \end{cases} \tag{16}$$

$$\gamma_1 = \begin{cases} \gamma_{1s} & \Theta < 1, \\ \gamma_{1n} & \Theta > 1, \end{cases} \tag{17}$$

$$\gamma_2 = \begin{cases} \gamma_{2s} & \Theta < 1, \\ \gamma_{2n} & \Theta > 1, \end{cases} \tag{18}$$

$$\alpha = \begin{cases} \alpha_s & \Theta < 1, \\ \alpha_n & \Theta > 1. \end{cases} \tag{19}$$

In general, while disregarding noise, the coupled differential equations (5) and (12) may have up to two different steady-state solutions. A superconducting steady state of the WL exists when $\Theta_\infty<1$ or, alternatively, when $E<E_s$, where $E_s=gC(T_c-T_0)/2\alpha_s\gamma_{2s}\hbar$. Similarly, a normal steady state of the WL's exists when $\Theta_\infty>1$ or, alternatively, when $E>E_n$, where $E_n=gC(T_c-T_0)/2\alpha_n\gamma_{2n}\hbar$.

In addition, the reflection coefficient S_{11} in steady state is in general given by[3]

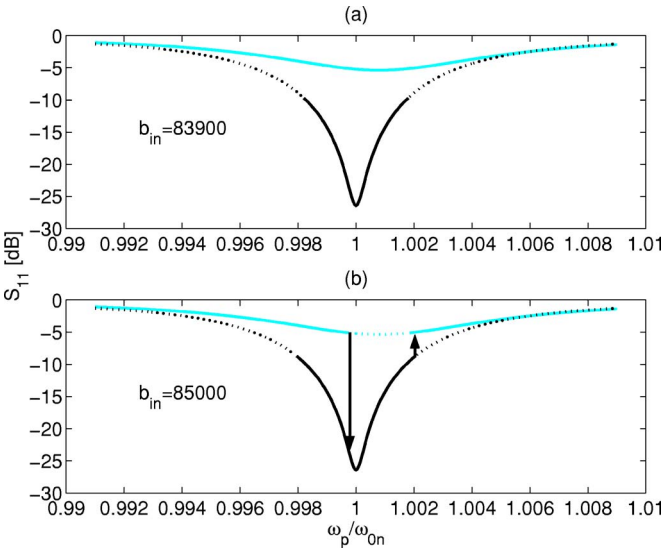

FIG. 12. (Color online). Simulated resonance response obtained by the hot-spot mechanism model. The different plots simulate the nonlinear behavior shown in Fig. 2. Panels (a) and (b) correspond to an increasing drive amplitude b^{in}. The solid lines represent valid steady-state solutions whereas the dotted lines represent invalid solutions. The black lines represent the normal WL solutions, whereas the cyan (gray) lines represent the superconducting WL solutions. The black arrows show the direction of the jumps in the different cases. The parameters that were used in the simulation are $\omega_{0s}/\omega_{0n}=1.0008$, $\gamma_{1n}/\omega_{0n}=2.5\times10^{-3}$, $\gamma_{1s}/\omega_{0n}=1.5\times10^{-3}$, $\gamma_{2n}/\omega_{0n}=2.75\times10^{-3}$, $\gamma_{2s}/\omega_{0n}=5\times10^{-3}$, $\alpha_n=0.8$, $\alpha_s=1$, $g=0.5$, and $\rho=10^{-10}$.

$$S_{11}=\frac{b^{out}}{b^{in}}=\frac{\gamma_2-\gamma_1-i(\omega_p-\omega_0)}{\gamma_2+\gamma_1-i(\omega_p-\omega_0)}. \tag{20}$$

B. Simulation results

Simulating the resonator system using this local heating WL model yields results which qualitatively agree with most of the nonlinear effects previously presented. In Sec. VI B 1 we simulate the main effects of Secs. III A–III D, whereas in Sec. VI B 2 we simulate and provide a possible explanation to the nonlinear features of Sec. III E.

1. Abrupt jumps and hysteretic behavior

In Fig. 12 we show a resonance response simulation result based on the hot-spot model, which simulates the abrupt jump exhibited in Fig. 2. The solid and dotted lines represent valid steady-state solutions of the system and invalid steady-state solutions, respectively, while the cyan (gray) and black colors represent superconducting WL solutions and normal WL solutions, respectively. In plot (a) the superconducting WL solution is valid in the normalized frequency span, and therefore the system follows this line shape without jumps. As we increase the amplitude drive b_{in} we obtain a result shown in plot (b). As the frequency is swept, jumps in the resonance response are expected to take place as the solution followed by the system (according to the initial conditions) becomes invalid. Thus in the forward sweep direction (as the frequency sweep of Fig. 2), we get two jumps indicated by black arrows on the figure. Similar to Fig. 2, the magnitudes of the jumps are unequal (the left jump is larger). This difference in the magnitude of the jumps is generally dependent on the relative position between the two resonance frequencies [Eq. (16)]. In the experiment, on the other hand, due to the metastability of the system in the hysteretic regime, it depends also on the frequency sweep rate. The simulation parameters used in the different phases are indicated in the figure captions.

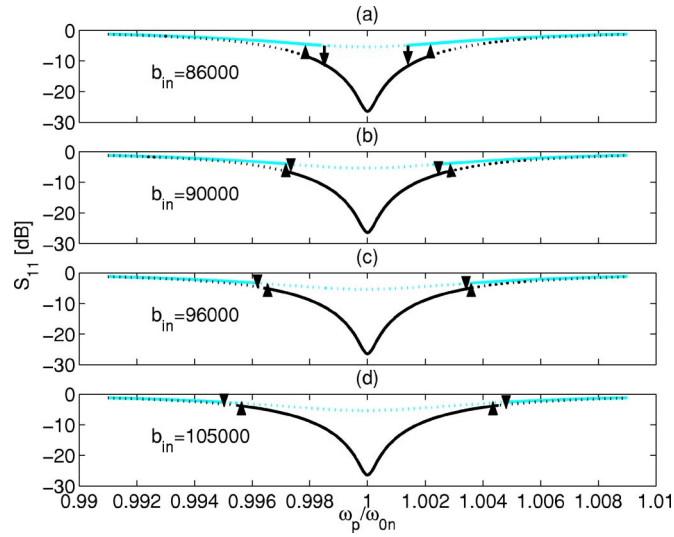

FIG. 13. (Color online). Simulated resonance response obtained by the hot spot mechanism model. Panels (a), (b), (c), and (d) correspond to an increasing drive amplitude b^{in}. The different plots simulate the nonlinear behavior shown in Fig. 3. The lines and symbols are the same as in Fig. 12. The parameters that were used in the simulation are $\omega_{0s}/\omega_{0n}=0.99989$, $\gamma_{1n}/\omega_{0n}=2.5\times10^{-3}$, $\gamma_{1s}/\omega_{0n}=1.5\times10^{-3}$, $\gamma_{2n}/\omega_{0n}=2.75\times10^{-3}$, $\gamma_{2s}/\omega_{0n}=5\times10^{-3}$, $\alpha_n=0.8$, $\alpha_s=1$, $g=0.5$, and $\rho=10^{-10}$.

The behavior of the frequency hysteresis loops exhibited in Fig. 3 is simulated in Fig. 13. The different plots exhibited in Fig. 13 correspond to the different phases shown in Fig. 3. In plot (a) the jumps in the forward direction (indicated by the arrows in that direction) occur at higher frequencies than the jumps in the backward direction, whereas in plot (b) corresponding to a higher drive amplitude b_{in} we show a case in which the left-side hysteresis loop vanishes as the two opposed jump frequencies coincide. If we increase b_{in} further, then at some drive amplitude as shown in plot (c), we get a similar case of vanishing hysteresis loop at the right side of the resonance response, whereas at the left side we get a frequency region where both the superconducting and normal WL solutions are invalid. In this instable region, transitions between the invalid solutions are expected, depending on the number of the sampling points, the sweep time, and the internal noise. However, due to this instability, the system is highly expected to jump "early" in each frequency direction, as it enters this region (at lower frequencies in the forward direction and at higher frequencies in the backward direction), thus leading to the observed change in the direction of the hysteresis loop. By increasing b_{in} further, one obtains a case in which both hysteresis loops are circulating

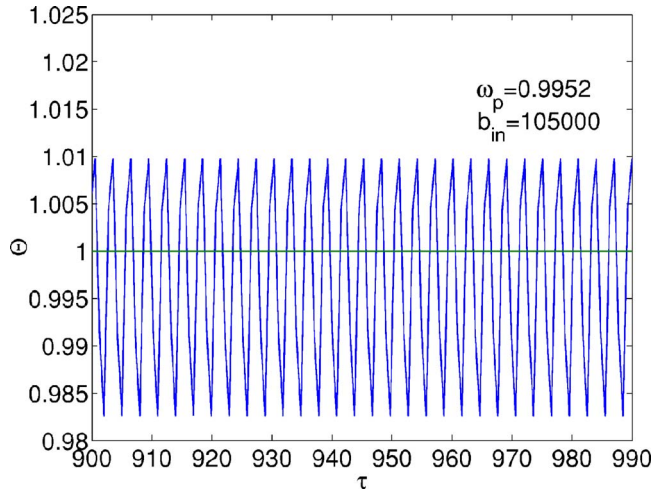

FIG. 14. (Color online). The dynamical solution of the coupled equations (5) and (12) at a normalized frequency of $\omega_p=0.9952$. The simulation parameters used are the same as those of Fig. 13(d).

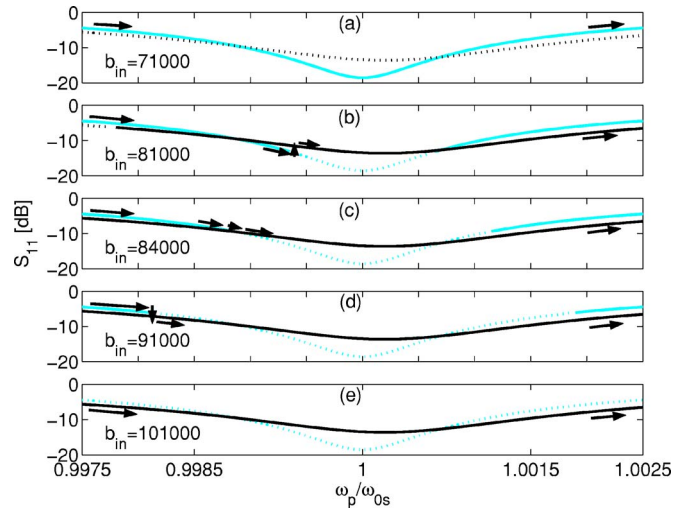

FIG. 15. (Color online). Simulated resonance response obtained by the hot-spot mechanism model. The different plots simulate the nonlinear behavior shown in Fig. 6. Panels (a), (b), (c), (d), and (e) correspond to an increasing drive amplitude b^{in}. The lines and symbols are the same as in Fig. 12. The simulation parameters used are $\omega_{0n}/\omega_{0s}=1.0002$, $\gamma_{1n}/\omega_{0s}=0.0029$, $\gamma_{1s}/\omega_{0s}=0.0019$, $\gamma_{2n}/\omega_{0s}=0.0019$, $\gamma_{2s}/\omega_{0s}=0.0015$, $\alpha_n=1$, $\alpha_s=0.8$, $g=0.5$, and $\rho=10^{-10}$.

in the opposite direction compared to plot (a).

Furthermore, the intermediate jump indicating instability, which appears at the left jump region of the last resonance curve in Fig. 3 (corresponding to −18.6 dBm), can be explained by this model as well. By solving the coupled equations (5) and (12) in the time domain for a single normalized frequency $\omega_p=0.9952$ (arbitrarily chosen in the left-side hysteresis region) and using the simulation parameters of Fig. 13(d), one obtains the oscillation pattern of the dimensionless temperature Θ as a function of the dimensionless time τ, which is shown in Fig. 14. The Θ oscillations indicating instability are between the superconducting and normal values, corresponding to $\Theta<1$ and $\Theta>1$, respectively.

As to the multiple-jump feature exhibited in Fig. 5, a straightforward generalization of the model may be needed in order to account for this effect. Such a generalization would include several WL's having a variation in their sizes and their critical current along the stripline, thus causing them to switch to the normal state at different drive currents (corresponding to different frequencies) and as a result induce more than two jumps in the resonance line shape.

2. Magnetic field dependence

In this subsection we show how the model of local heating of WL's can also account for the nonlinear dynamics of the resonance line shape observed under an applied magnetic field.

To this end, we show in Fig. 15 a simulation result based on the WL local heating model, which regenerates qualitatively the nonlinear behavior of the resonance line shape of B2 under a constant magnetic field (presented in Fig. 6). At low drive amplitude b_{in}, only the superconducting WL steady-state solution exists, and thus no jump occurs as one sweeps the frequency [plot (a)]. Increasing the drive amplitude b_{in} [plot (b)] causes the superconducting WL solution to become invalid in the center frequency region; thus, the resonance response jumps upward (as the system reaches the invalid region) and stabilizes on the normal WL steady-state solution, as indicated by arrows in the plot. By increasing the drive amplitude further [plot (c)] one gets an intersection point where a smooth transition (without a jump) is expected to occur between the valid superconducting WL solution and the valid normal one, whereas in plot (d), where we have increased b_{in} further, a downward jump in the resonance response occurs as the valid normal WL solution lies below the invalid superconducting WL solution. Finally in plot (e), corresponding to a much higher drive, only the normal WL steady-state solution exists (within the frequency span), and therefore there are no jumps in the resultant curve.

Another measurement which can be explained using the WL model is the measurement shown in Fig. 7, where the left-side jump vanishes as the magnetic field increases above some low-magnetic-field threshold. This result can be explained in the following manner. Increasing the applied dc magnetic field would increase the screening supercurrent flowing in the film and the local heating of the WL. As the local heating exceeds some threshold, the superconducting WL solution would become invalid (within the same frequency span), and consequently, the system would only follow the normal WL solution without apparent jumps.

VII. SUMMARY

In attempt to investigate and manifest nonlinear effects in superconducting microwave resonators, several superconducting NbN resonators employing different layouts, but similar sputtering conditions, have been designed and fabricated. The resonance line shapes of these NbN resonators having a very low onset of nonlinearity, several orders of magnitude lower than other reported nonlinearities,[13,45,46] exhibit some extraordinary nonlinear dynamics. Among the nonlinearities observed while applying different measure-

ment configurations are abrupt metastable jumps in the resonance line shape, hysteresis loops changing direction, multiple jumps, vanishing jumps, and jumps changing direction. These effects are hypothesized to originate from weak links located at the boundaries of the columnar structure of the NbN films. This hypothesis is fully consistent with SEM micrographs of these films and generally agrees with the extrinsiclike behavior of these resonators. To account for the various nonlinearities observed, a theoretical model assuming local heating of weak links is suggested. Furthermore, simulation results employing this model are shown to be in a very good qualitative agreement with measurements.

Such strong sensitive nonlinear effects reported herein may be utilized in the future in a variety of applications, ranging from qubit coupling in quantum computation to signal amplification[47] and to the demonstration of some important quantum effects in the microwave regime.[3,48]

ACKNOWLEDGMENTS

E.B. would especially like to thank Michael L. Roukes for supporting the early stage of this research and for many helpful conversations and invaluable suggestions. Very helpful conversations with Oded Gottlieb, Gad Koren, Emil Polturak, and Bernard Yurke are also gratefully acknowledged. This work was supported by the German Israel Foundation under Grant No. 1-2038.1114.07, the Israel Science Foundation under Grant No. 1380021, the Deborah Foundation, and the Poznanski Foundation.

*Electronic address: baleegh@tx.technion.ac.il

[1] R. Movshovich, B. Yurke, P. G. Kaminsky, A. D. Smith, A. H. Silver, R. W. Simon, and M. V. Schneider, Phys. Rev. Lett. **65**, 1419 (1990).
[2] B. Yurke, P. G. Kaminsky, R. E. Miller, E. A. Whittaker, A. D. Smith, A. H. Silver, and R. W. Simon, IEEE Trans. Magn. **25**, 1371 (1989).
[3] B. Yurke and E. Buks, quant-ph/0505018 (unpublished).
[4] E. Buks and B. Yurke, Phys. Rev. A **73**, 023815 (2006).
[5] I. Siddiqi, R. Vijay, F. Pierre, C. M. Wilson, M. Metcalfe, C. Rigetti, L. Frunzio, and M. H. Devoret, Phys. Rev. Lett. **93**, 207002 (2004).
[6] I. Siddiqi, R. Vijay, F. Pierre, C. M. Wilson, L. Frunzio, M. Metcalfe, C. Rigetti, R. J. Schoelkopf, M. H. Devoret, D. Vion, and D. Esteve, Phys. Rev. Lett. **94**, 027005 (2005).
[7] P. J. Burke, R. J. Schoelkopf, D. E. Prober, A. Skalare, B. S. Karasik, M. C. Gaidis, W. R. McGrath, B. Bumble, and H. G. LeDuc, Appl. Phys. Lett. **85**, 1644 (1999).
[8] R. Sobolewski, A. Verevkin, G. N. Gol'tsman, A. Lipatov, and K. Wilsher, IEEE Trans. Appl. Supercond. **13**, 1151 (2003).
[9] I. Chiorescu, Y. Nakamura, C. J. P. M. Harmans, and J. E. Mooij, Science **299**, 1869 (2003).
[10] T. Dahm and D. J. Scalapino, J. Appl. Phys. **81**, 2002 (1997).
[11] Z. Ma, E. de Obaldia, G. Hampel, P. Polakos, P. Mankiewich, B. Batlogg, W. Prusseit, H. Kinder, A. Anderson, D. E. Oates, R. Ono, and J. Beall, IEEE Trans. Appl. Supercond. **7**, 1911 (1997).
[12] R. B. Hammond, E. R. Soares, B. A. Willemsen, T. Dahm, D. J. Scalapino, and J. R. Schrieffer, J. Appl. Phys. **84**, 5662 (1998).
[13] C. C. Chin, D. E. Oates, G. Dresselhaus, and M. S. Dresselhaus, Phys. Rev. B **45**, 4788 (1992).
[14] L. F. Cohen, A. L. Cowie, A. Purnell, N. A. Lindop, S. Thiess, and J. C. Gallop, Supercond. Sci. Technol. **15**, 559 (2002).
[15] A. L. Karuzskii, A. E. Krapivka, A. N. Lykov, A. V. Perestoronin, and A. I. Golovashkin, Physica B **329-333**, 1514 (2003).
[16] Z. Ma, E. D. Obaldia, G. Hampel, P. Polakos, P. Mankiewich, B. Batlogg, W. Prusseit, H. Kinder, A. Anderson, D. E. Oates, R. Ono, and J. Beall, IEEE Trans. Appl. Supercond. **7**, 1911 (1997).
[17] J. Wosik, L.-M. Xie, J. H. Miller, Jr., S. A. Long, and K. Nesteruk, IEEE Trans. Appl. Supercond. **7**, 1470 (1997).
[18] B. A. Willemsen, J. S. Derov, J. H. Silva, and S. Sridhar, IEEE Trans. Appl. Supercond. **5**, 1753 (1995).
[19] A. M. Portis, H. Chaloupka, M. Jeck, and A. Pischke, Supercond. Sci. Technol. **4**, 436 (1991).
[20] S. J. Hedges, M. J. Adams, and B. F. Nicholson, Electron. Lett. **26**, 977 (1990).
[21] J. Wosik, L.-M. Xie, R. Grabovickic, T. Hogan, and S. A. Long, IEEE Trans. Appl. Supercond. **9**, 2456 (1999).
[22] D. E. Oates, M. A. Hein, P. J. Hirst, R. G. Humphreys, G. Koren, and E. Polturak, Physica C **372-376**, 462 (2002).
[23] M. A. Golosovsky, H. J. Snortland, and M. R. Beasley, Phys. Rev. B **51**, 6462 (1995).
[24] S. K. Yip and J. A. Sauls, Phys. Rev. Lett. **69**, 2264 (1992).
[25] D. E. Oates, H. Xin, G. Dresselhaus, and M. S. Dresselhaus, IEEE Trans. Appl. Supercond. **11**, 2804 (2001).
[26] B. B. Jin and R. X. Wu, J. Supercond. **11**, 291 (1998).
[27] A. V. Velichko, D. W. Huish, M. J. Lancaster, and A. Porch, IEEE Trans. Appl. Supercond. **13**, 3598 (2003).
[28] J. Halbritter, J. Appl. Phys. **68**, 6315 (1990).
[29] B. Abdo, E. Segev, Oleg Shtempluck, and E. Buks, IEEE Trans. Appl. Supercond. (to be published), cond-mat/0501114.
[30] J. H. Oates, R. T. Shin, D. E. Oates, M. J. Tsuk, and P. P. Nguyen, IEEE Trans. Appl. Supercond. **3**, 17 (1993).
[31] H. Xin, D. E. Oates, G. Dresselhaus, and M. S. Dresselhaus, J. Supercond. **14**, 637 (2001).
[32] R. Whiteman, J. Diggins, V. Schöllmann, T. D. Clark, R. J. Prance, H. Prance, and J. F. Ralph, Phys. Lett. A **234**, 205 (1997).
[33] H. Prance, T. D. Clark, R. Whiteman, R. J. Prance, M. Everitt, P. Stiffel, and J. F. Ralph, Phys. Rev. E **64**, 016208 (2001).
[34] R. J. Prance, R. Whiteman, T. D. Clark, H. Prance, V. Schöllmann, J. F. Ralph, S. Al-Khawaja, and M. Everitt, Phys. Rev. Lett. **82**, 5401 (1999).
[35] J. S. Aldridge and A. N. Cleland, Phys. Rev. Lett. **94**, 156403 (2005).
[36] H. A. Kramers, Physica (Amsterdam) **7**, 284 (1940).
[37] D. M. Sheen, S. M. Ali, D. E. Oates, R. S. Withers, and J. A. Kong, IEEE Trans. Appl. Supercond. **1**, 108 (1991).
[38] S. Isagawa, J. Appl. Phys. **52**, 921 (1980).

[39] Y. M. Shy, L. E. Toth, and R. Somasundaram, J. Appl. Phys. **44**, 5539 (1973).
[40] M. W. Johnson, A. M. Herr, and A. M. Kadin, J. Appl. Phys. **79**, 7069 (1996).
[41] A. M. Kadin and M. W. Johnson, Appl. Phys. Lett. **69**, 3938 (1996).
[42] K. Weiser, U. Strom, S. A. Wolf, and D. U. Gubser, J. Appl. Phys. **52**, 4888 (1981).
[43] C. W. Gardiner and M. J. Collett, Phys. Rev. A **31**, 3761 (1985).
[44] A. VI. Gurevich and R. G. Mints, Rev. Mod. Phys. **59**, 941 (1987).
[45] P. P. Nguyen, D. E. Oates, G. Dresselhaus, M. S. Dresselhaus, and A. C. Anderson, Phys. Rev. B **51**, 6686 (1995).
[46] A. Andreone, A. Cassinese, A. Di Chiara, M. Lavarone, F. Palomba, A. Ruosi, and R. Vaglio, J. Appl. Phys. **82**, 1736 (1997).
[47] B. Abdo, E. Segev, O. Shtempluck, and E. Buks, Appl. Phys. Lett. **88**, 022508 (2006).
[48] B. Abdo, E. Segev, O. Shtempluck, and E. Buks, cond-mat/0501236 (unpublished).